ARTICLE IN PRESS

INTERNATIONAL JOURNAL OF HYDROGEN ENERGY XXX (XXXX) XXX

Available online at www.sciencedirect.com

ScienceDirect

journal homepage: www.elsevier.com/locate/he

State machine-based architecture to control system processes in a hybrid fuel cell electric vehicle

Ali Molavi [a,*], Attila Husar [a], Hampus Hjortberg [b], Niclas Nilsson [b], Markus Kogler [c], Juan Sanchez Monreal [d], Yousif Eldigair [e,a], Maria Serra Prat [a]

[a] Institut de Robotica I Informatica Industrial, CSIC-UPC, Barcelona, Spain
[b] PowerCell, Gothenburg, Sweden
[c] AVL, Graz, Austria
[d] German Aerospace Center (DLR), Institute of Engineering Thermodynamics, Pfaffenwaldring 38-40, 70569, Stuttgart, Germany
[e] Brose Fahrzeugteile SE & CO., Würzbrug, Germany

HIGHLIGHTS

- State machine-based supervisory controller for fuel cell system is designed.
- The designed control structure is implemented in a prototype hydrogen-based vehicle.
- The controller comprises: State Machine, Setpoint Generator, Power Limit Calculator.
- The proposed control structure handles the startup and shutdown process of PEMFC.
- Minimizing stack degradation by implementing a fuel cell power limit calculator.

ARTICLE INFO

Article history:
Received 29 October 2022
Received in revised form
3 July 2023
Accepted 5 July 2023
Available online xxx

Keywords:
Supervisory controller
PEM fuel cell
Hydrogen based electric vehicle
State machine
Optimal setpoint generator

ABSTRACT

This paper presents the development and implementation of a system supervisory controller in a hydrogen-based fuel cell electric vehicle. The controller's primary function is to ensure the safe control of the fuel cell system processes while facilitating coordination among various subsystems, including the balance of plant subsystems, vehicle control unit, diagnosis unit, and powertrain. The supervisory controller comprises of three primary parts: a State Machine, an Optimal Setpoint Generator, and a Power Limit Calculator. The State Machine, which serves as the central part of the supervisory controller, coordinates the fuel cell system's different operational states, including the complex processes of start-up and shutdown. To maximize the fuel cell system's efficiency and minimize the stack's degradation, the Optimal Setpoint Generator produces the subsystem's setpoints by solving an optimization problem and considering the manufacturer's requirements. The Power Limit Calculator assesses the stack's power output capability and calculates the current setpoint for the DC/DC converter. It then provides this data to the Energy Management System (EMS), which oversees the distribution of power between the fuel cell system and the batteries. The proposed fuel cell system supervisory controller is verified using the Worldwide Harmonized Light Vehicles Test Cycles (WLTC) in a real-world car. The designed control structure is implemented in a prototype hydrogen-based electric car at

* Corresponding author.
E-mail address: ali.molavi@upc.edu (A. Molavi).
https://doi.org/10.1016/j.ijhydene.2023.07.039

both PowerCell and CEVT facilities under the framework of the INN-BALANCE Horizon 2020 European project.

Introduction

Fuel cell electric vehicles have been increasingly under development due to their ability to provide extended driving ranges at zero-emission [1]. However, this type of vehicle faces several challenges. The lifetime and durability of a fuel cell system is a key point in the development of fuel cell vehicles, and it is a critical factor for end-user acceptance [2]. In automotive applications, the fuel cell systems have to be able to adapt to a wide range of operating conditions given by start-up and shutdown processes, sudden load changes, or varying power levels [3,4]. The durability and lifetime of the stack are affected by its operating conditions (temperature, humidity, pressure, mass flow rate, etc.) during drive cycles, idling, start-up, and shutdown procedures [5]. To enhance the durability and lifespan of the fuel cell system, various types of optimization problems are defined, including energy management optimization, operating condition optimization, and system sizing optimization.

The rate of change in the load is often faster than the dynamic happening inside the fuel cell. As a result, fuel cell systems are often used alongside other energy storage sources like batteries or ultracapacitors in hybrid electric vehicles [6]. Currently, there are five distinct types of fuel-cell hybrid electric vehicles being developed, each with its own unique topological structure. These include fully fuel-cell (FC), FC combined with a battery, FC combined with ultracapacitors (UC), FC combined with both a battery and UC, and FC combined with other energy sources such as flywheels or solar panels (SPVs). The implementation and control simplicity, energy recovery capability, energy density, and cost of each of these structures come with their own advantages and disadvantages [7]. In situations where there is a high demand of power, the battery and ultracapacitors can come into play to recover excess energy and provide power alongside the fuel cells to ensure the system continues to receive sufficient power [6].

Distributing the power between these energy sources to accomplish important objectives such as lowering energy usage and extending fuel cell system lifespan is done through energy management strategies (EMSs). The most common EMSs strategies used nowadays include Rule-based [8], offline optimization-based [9], online optimization-based [10], and learning-based [11]. Alongside power allocation between multiple energy sources, co-optimization and cooperative controls are employed to optimize the energy consumption, while taking into account the influence of other factors, such as traffic environment and speed planning [12], sizing [13]. To consider the effect of performance drifts owing to aging and operating condition, a state machine-based adaptive EMS was proposed in Ref. [14]. A Kalman filter (KF) was used to keep track of the performance drifts.

The load cycle in automotive applications causes a cyclic change in the stoichiometric ratio and pressure of the supplied gases, which makes the gas starvation very likely. Additionally, the electrochemically generated water and heat inside the fuel cell vary with changes in load, creating an internal environment of thermal/humidity cycling that radically accelerates catalyst aging and mechanical degradation of components [15]. Therefore, operating in the optimal operation condition is very important to diminish these effects.

In terms of operating conditions, researchers have published many works focused on the optimization of operating conditions for automotive applications. In Ref. [3], a quasi-steady fuel cell model of the fuel cell system integrated into the vehicle model was developed and used to optimize the air pressure and mass flow rate to maximize system efficiency. Another strategy is proposed in Ref. [16] to maximize the system performance. However, the pressure is assumed to be constant, and the consumption loss is not considered. A model reference adaptive control was presented in Ref. [17] to maximize the efficiency considering the optimal oxygen ratio. However, the temperature and humidity ratio are assumed to be constant and there is no experimental implementation. In Ref. [18], the optimal operating temperature corresponding to the point with the fuel cell's largest efficiency is obtained through a fuel cell based truck test bench, and a model predictive control was proposed to control the temperature. The Particle Swarm Optimization (PSO) algorithm was proposed in Ref. [19] to optimize the operating conditions and design parameters of a high-temperature PEMFC-based vehicle. However, the algorithm is not applicable in real vehicle due to its high computation time, and the optimal conditions for different load currents were not reported.

Besides the dynamic changes in load and the need to work under optimal operating conditions, the working state of the automotive fuel cell imposes other conditions, such as start-up and shutdown, which can cause degradation and decrease the useful life of the PEMFC. The start-stop state contributes about 33%to the degradation of PEMFC during operation [20]. Therefore, the application of strategies to mitigate the degradation of the stack is crucial for PEMFC systems, particularly for transportation systems that experience frequent start-up and shutdown events throughout their lifetimes.

One of the challenges in the start-up and shutdown procedure is the freeze start-up and shutdown. Starting a fuel cell at sub-freezing temperatures has always been a challenge due to the freezing of the water produced. Ice formation inside the stack blocks the cathode channel, preventing the stack from producing power, and causing start-up to fail. A successful cold start requires the cell temperature raises above the freezing point before the cathode catalyst layer becomes blocked with ice [21]. The cold start strategies can be divided into self-cold start and assisted cold start, according to the heating sources. The self-cold start relies entirely on the heat generated by the electrochemical reaction, which is usually achieved by regulating the load current, i.e., galvanostatic mode [22]. However, due to low water content during the start-up, the stack cannot support high current density and the self-heating capability of the stack may not be sufficient. Therefore, alternative strategies including the potentiostatic mode [23], ramping the load current [24] and regulating the output power [25] were proposed. The assisted cold start-up, in which supplementary heat is applied to overcome the shortcomings of the cold start-up, can effectively address the challenges related to self-cold start-up. Montaner Ríos et al. in Ref. [26] proposed a coolant heating strategy to heat a 4 kW PEMFC. They used the cooling subsystem to heat the stack during the start-up. Eliminating the water produced due to reaction is crucial to have a successful start-up and shutdown. In Ref. [27], an effective gas purge as a key step to remove the residual water inside the cell and subsequently prevent the ice formation in the cathode catalyst layer was proposed. Excluding the start-up and shutdown issues, there are certain conditions, such as ascending or acceleration, where the fuel cell operates under high power conditions for short periods. Due to the impact of compressor dynamic and gas inertia, there is a risk of gas starvation, which is harmful to the fuel cell stack [28]. This work suggests a strategy in which the current of the fuel cell, which is equivalent to the DC/DC converter current setpoint, is determined by considering the incoming airflow at the stack inlet. This approach helps to minimize the likelihood of the gas starvation. As aforementioned in Ref. [3], and [15–26], the majority of existing experimental studies mainly focus on laboratory scale fuel cells and there is a lack of adequate documentation regarding the implementation of PEMFC application in real-world vehicles. In particular, there is the scarcity of research with a comprehensive control unit for fuel cell system that encompasses all necessary components to enhance fuel cell durability and system reliability in an automotive application. Additionally, the implementation of such a control unit in a real vehicle is crucial for the practicality and usefulness of the work.

The main objective of this paper is to design and implement a fuel cell system supervisory controller (FCSSC) based on a state machine architecture for a Fuel Cell Electric Vehicle (FCEV). The considered Fuel Cell System (FCS) is a complex system with multiple states of operation. This includes the Start-up, Run, Shut-down and Idle states, which have been identified as the states of a State Machine (SM). Furthermore, the FCS consists of several subsystems, namely the cathode, anode, thermal subsystems, and the DC/DC converter, which all have distinct operational modes. In each specific state of the FCS, the subsystems can operate in various modes of operation. Therefore, a control structure is necessary to coordinate these subsystems and the stack in the different FCS operation states and the operation modes of the different subsystems.

The main contributions and parts of this work are summarized as follows:

- Design a FCSSC using a State machine to control all the fuel cell system processes in an automotive application.
- Design an offline optimal setpoint generator that calculates the setpoints of the subsystems controlled variables in a way that enhances efficiency while considering all manufacturer limitations to minimize degradation during the Run state.
- Minimizing the damage to the fuel cell stack, particularly in the high power demanded conditions such as ascending and acceleration. This is achieved by estimating the immediate and future fuel cell stack power capabilities. This estimation is based on the stack variables measurements, and it is fed to the vehicle's energy management system (EMS). Furthermore, the DC/DC current setpoint is calculated based on the available air mass flow at the inlet of the stack to prevent air starvation or high-power extraction.
- Propose a start-up strategy that combines the benefits of self-cold start, which involves the capability to function in either potentiostatic or galvanostatic mode, and coolant heating assisted cold start. Furthermore, the compressor air blowing is used in the start-up and shutdown to remove the generated water and prevent the formation of ice.
- As the purpose of INN-BALANCE project was to develop advanced balance-of-plant components (BoP) for current generation of fuel cell-based vehicles, the designed FCSSC was implemented and tested in the real prototype vehicle in PowerCell and CEVT facilities. The INN-BALANCE consortium was composed of industrial actors (BRO, AVL, CEVT, AYE), research and technology organizations (DLR, S2i), SMEs with research capabilities (CEL, PCS) and a higher research institution (UPC).

The paper is organized into the following sections. Section Fuel cell system description is assigned to the description of the fuel cell system. In section Supervisory controller design, the fuel cell system supervisory controller is described, which includes optimal setpoint generator, state machine, and power limit calculator. Section Automotive run state test and experimental results is dedicated to the experimental results of the prototype electric vehicle in terms of demanded load tracking and the balance of plant performance. Software implementation guidelines are described in section Software implementation guidelines. The main conclusions and key results are summarized in section Conclusion.

Fuel cell system description

The fuel cell system implemented in this work is shown in Fig. 1. It includes four auxiliary subsystems, i.e., anode, cathode, thermal, and power electronic subsystems. The hydrogen is stored in a pressurized tank and is delivered to the stack anode channel through the anode subsystem. The unutilized hydrogen, which exits the stack, has to be recovered and recirculated to increase the hydrogen utilization rate and overall FCS efficiency. An ejector-injector in the re-circulation path is used for re-circulation implementation, and to maintain a more uniform hydrogen concentration in the stack. The anode subsystem is outfitted with a water separator and a purge valve to remove the accumulated liquid water, and the

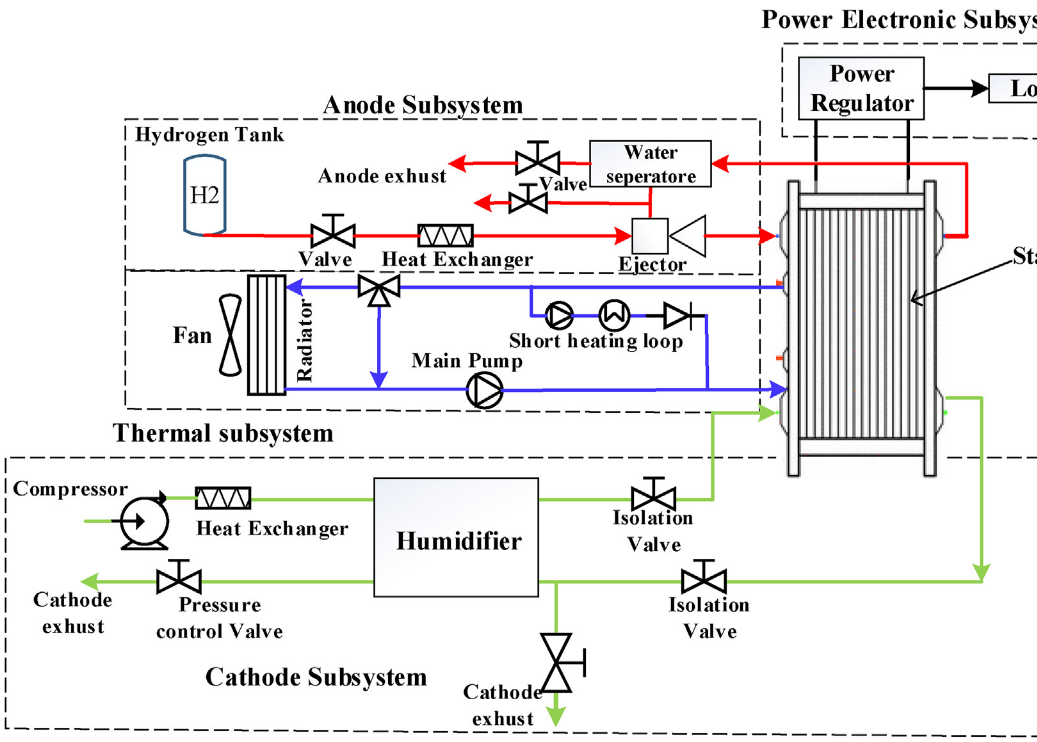

Fig. 1 — Fuel cell stack and the balance of plant auxiliary subsystems.

nitrogen diffused through the membrane from the cathode to the anode side. A pre-heating hydrogen heat exchanger is integrated into the anode module. The purpose is to avoid condensation when cold dry hydrogen is mixed with warm humid nitrogen and hydrogen from the stack outlet. Partner AVL[1] developed the anode subsystem. The cathode subsystem is in charge of delivering the demanded air flow to run the fuel cell. It is equipped with a turbo-compressor with air-bearings, which, compared to conventional oil-bearings, guarantees pure and uncontaminated air supply. Furthermore, by using gas-bearings, frictional losses are reduced, and the lifetime of the compressor is extended. To ensure the proper functioning of the fuel cell stack, the pressure, mass flow, temperature and humidity of the air to be fed into the stack are constantly monitored and controlled. Partner BROSE[2] coordinated the development of the cathode subsystem. The operating stack temperature has to be kept in the proper range to maintain optimum electrochemical reactions and keep the integrity of the PEMFC stack material. The thermal subsystem provides a coolant flow to remove the generated heat through a radiator. In addition, the thermal subsystem is equipped with a heating circuit including a pump and a heater to heat the stack in the subfreezing start-up. Partner DLR[3] developed the thermal subsystem. Finally, the power electronic subsystem is in charge of the electric power conditioning and is developed by CEVT[4].

[1] AVL List GmbH, Engineering Service Provider.
[2] Brose Mechatronics, Germany.
[3] German Aerospace Center (DLR), Institute of Engineering Thermodynamics, Stuttgart, Germany.
[4] China Euro vehicle technology.

Supervisory controller design

In this section, a novel FCSSC is proposed and described. Supervisory controllers distribute the system's global requests to particular requests necessary from individual subsystems or components of the system equipment set. The individual demands are translated into the setpoints of the local controllers [29]. The proposed fuel cell supervisory controller integrated with the rest of the vehicle propulsion system is shown in Fig. 2. The fuel cell hybrid electric vehicle's overall control system architecture is divided into different layers. The highest level of control is the Vehicle Control Unit. The second level, which is the focus of this work, is the FCSSC. It consists of three principal parts, namely the State Machine (SM), Optimal Setpoint Generator (OPSG), and Power Limit Calculator (PLC). The FCSSC developed in this work is a hybrid control system because the statemachine is a discrete event control system that decides when to activate the distinct operating states and sub-states, and the OPSG is a control system in charge of the continuous generation of proper setpoints for the subsystem's local controllers. The state machine is developed with Stateflow, and the continuous control system is implemented as an optimal setpoint generator linked to the local controllers. Finally, the supervisory controller contains a Power Limit Calculator part that estimates the available stack power. The supervisory controller receives all the information from the input wrapper, which collects 33 input signals. These signals include commands from the Vehicle Control Unit (VCU), estimation results from the observer, and the diagnostic results from the diagnostic unit. The supervisory controller uses the collected data to automatically coordinate the subsystems, establishes local controller setpoints, determines DC/DC

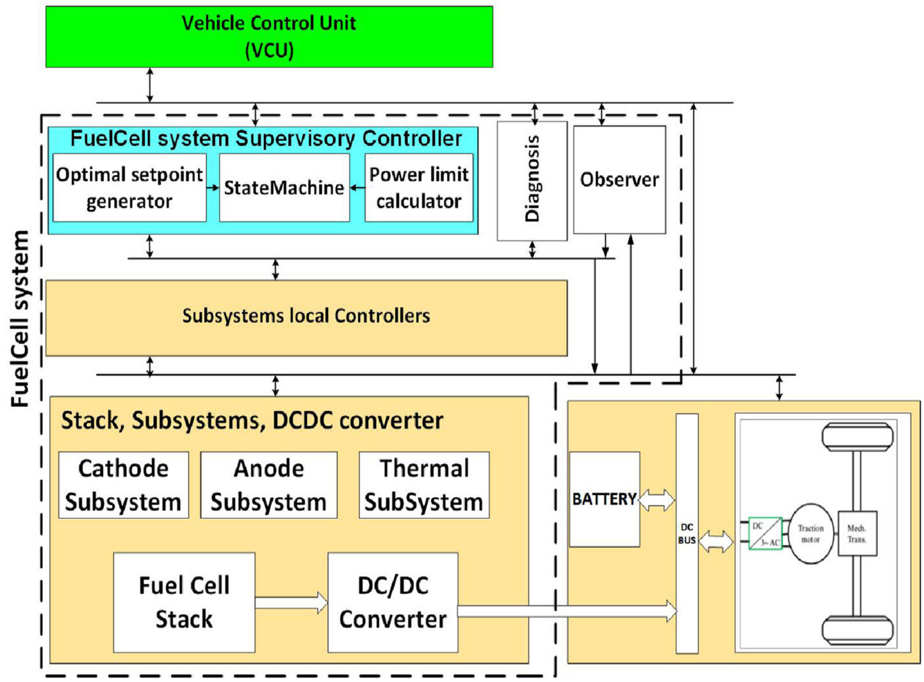

Fig. 2 — Control Layered structure implemented in this project that shows the hierarchy of control unit in three layers, namely vehicle control unit, fuel cell system supervisory controller, and the subsystems local controllers.

converter current setpoint, and estimates stack available power information for the VCU. The diagnosis unit is in charge of diagnosing hardware failure such as sensors failure, compressor errors, etc. The third level includes the ancillary subsystem's local controllers, i.e., anode, cathode, and thermal subsystem's controllers. Each subsystem controller (SSC) is programmed with local control algorithms to achieve the set-points received from the FCSSC at the upper level.

Functionality of the state machine

A complex system as a vehicle has different states of operation, corresponding to different functions. There are ten operation states for the fuel cell system in this automotive application, which include: Initial, Failsafe, Standby, Refueling, Service mode, Start-up, Run, Min Power, Normal shutdown, and Fast shutdown. The overall scheme of the proposed SM is shown in Fig. 3. During each operation state, the SM manages the activation of the different subsystems' modes of operation through the protocol numbers. The outputs of the SM are the protocol numbers, subsystems' set-points, and the error detection flags implemented inside SM.

Protocol numbers and status numbers

The SM uses protocol numbers and status numbers to communicate with the subsystems. The numerical values of the protocol/status numbers refer to specific modes of operation of the different subsystems, and the protocol numbers and the status numbers use the same numerical values. The different operation modes of the four subsystems and the assigned protocol numbers to their different operation modes are listed in Table 1. The supervisory controller commands the different subsystems to change their modes by sending them the protocol number that corresponds to the desired mode. By receiving the command, the subsystems respond by changing their operation mode, and subsequently, return the updated status number to SM. An example is explained in section Automotive run state test and experimental results.

SM cycle

The overall scheme of the SM is shown in Fig. 3. In each state or substate of the SM, this state or substate is in charge of determining all the SM outputs. The fuel cell supervisory control unit is turned on when the vehicle is started and the onboard computer turns on. The SM starts in the initial state named ‘Initialization’, and all subsystems remain inactive. If the different subsystems report their successful initialization, the SM moves to the ‘Standby’ state, and waits until the ‘Run-Requested’ is activated by the VCU. In the ‘Standby’ state, all the subsystems are still off except the thermal subsystem, where the main pump is turned on. This pump cleans up any ions in the coolant liquid inside the stack by circulating the coolant liquid in the thermal loop. Once the ‘Run-Requested’ is activated, the SM moves to the next state, where the ‘Start-up’ procedure starts. In the ‘Start-up’ state, the various subsystems are activated based on the defined procedure. Once the ‘Start-up’ procedure has finished, the ‘Run’ state starts only if the “Run-Requested” is still active. In case of a need to stop the vehicle, the ‘Minimum Power’ state for the fuel cell system is activated. This state allows the system to return to the “Run” state when the stop corresponds to the instance of a red light, or it can proceed to a ‘Normal Shutdown'as shown in Fig. 3. If the system's state changes to ‘Normal Shutdown’, the subsystems have to be turned off in an orchestrated manner by receiving ordered protocol numbers to avoid damage to the fuel cell stack. The fuel cell system state switches to ‘Standby’

Please cite this article as: Molavi A et al., State machine-based architecture to control system processes in a hybrid fuel cell electric vehicle, International Journal of Hydrogen Energy, https://doi.org/10.1016/j.ijhydene.2023.07.039

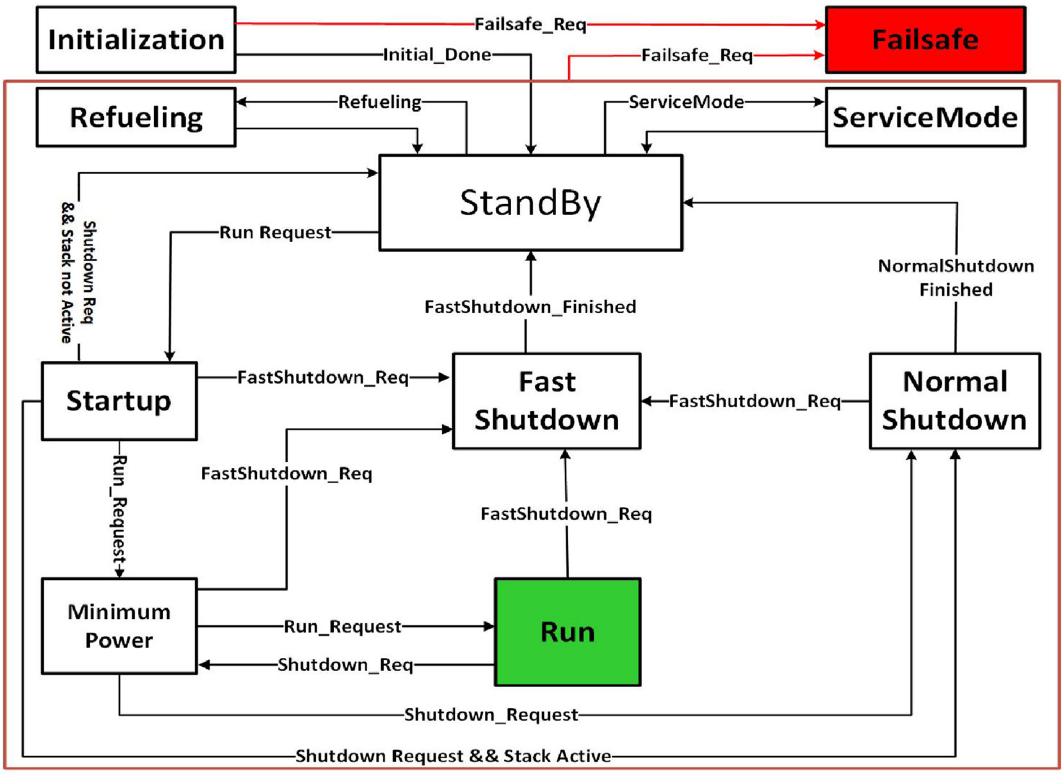

Fig. 3 – Overall scheme of the proposed state machine, including the fuel cell system states and transient requirement conditions between states.

Table 1 – Subsystem operation's modes and their corresponding protocol numbers and status numbers.

Cathode Operation Modes	Protocol and Status number	Thermal Operation Modes	Protocol and Status number	Anode Operation Modes	Protocol and Status number	DC/DC Operation Modes	Protocol and Status number
Off	0	Off	0	Off	0	Standby	0
Bypass Humidification	1	Heating loop without heater	1	Start-up	1	Galvanostatic	1
Start Compressor Bypass air	2	Heating loop with heater	2	Run	2	Potentiostatic	2
Min flow	3	Cooling loop	3	Shutdown	3	Passive	5
Run	4	Cooling Loop for isolation	4			Error	15
Max flow	5						

state when the Shutdown is finished. In the case of a malfunction in one of the subsystems or components, the 'Failsafe' state is triggered, and the whole system is depowered. The 'Failsafe' state has the highest priority among the other states of operation. In the next section, the Start-up and Shutdown procedures are explained.

Start-up procedure

During the 'Start-up' procedure, the SM sends the protocol numbers and setpoints to the subsystem controllers to start the different subsystems. The SM gets feedback from the subsystems with the sensors and the status variables. The start-up procedure is shown in Fig. 4(a). During start-up, the SM triggers the activation of various modes of operation in the subsystems as it progresses through different substates within the start-up state. The condition to transit from one substate for example, 'start compressor bypass' to the next substate, 'compressor min flow', is to receive a status number from the cathode subsystem that confirms the compressor started successfully; otherwise, the SM remains in the previous substate until a timeout is reached and the 'Failsafe' is activated. The status numbers are shown with $SN\_X = k$. The indexes k and X are the status number value k for the subsystem X which are listed in Table 1. $SN\_Ca = 2$ means that the cathode subsystem has returned successfully the status number 2. Fig. 5(a) shows the activation signals for the first 40 s of a 'Normal Start-up' in the real vehicle. It shows the change in the protocol number of the different subsystems to do a successful start-up. In addition, it shows two locally controlled measured variables, which are the mass flow of air and the inlet coolant temperature. The mass flow of the compressor increases when the protocol number of the cathode changes from 0, then decreases to a setpoint value for protocol number = 4 at t = 14 s. In this test, the stack

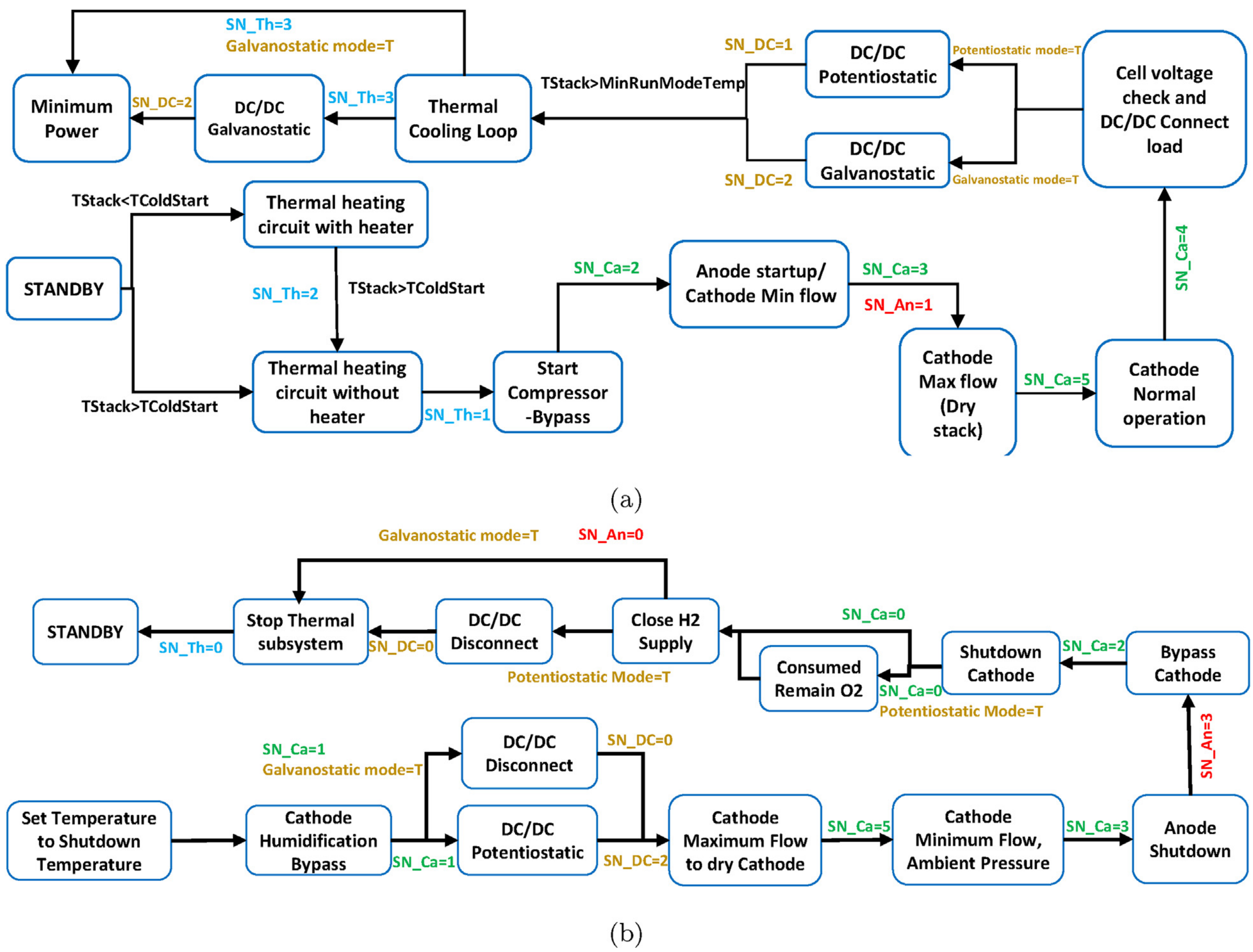

Fig. 4 – (a) Start-up procedure sub-state machine. (b) Shutdown procedure sub-state machine, and the transient conditions between sub-states as were explained in section SM cycle.

temperature is $T\_stack > 33°C$ and the 'heating loop without heater' is activated in the thermal subsystem with protocol number = 1. The 'cooling loop' is activated at t = 14 s and the temperature of the coolant decreases due to the volume of water inside the radiator. The temperature starts to increase at t = 23 s due to the occurring electrochemical reaction inside the stack, and it continues to reach a defined temperature setpoint. The setpoints of these variables are defined by the SM. In the case of low temperature, the proposed strategy in this work is to activate the thermal subsystem mode, which applies extra heat and the assisted cold start-up is proceeded. This action is done in the second step of the start-up procedure by activating the 'Thermal heating circuit with heater'. The mode 'Cathode Max flow (Dry stack)' is enabled by the cathode subsystem to achieve the maximum flow rate that eliminates the produced water as well as prevents the formation of ice. Based on the real-world tests conducted on a prototype vehicle, it has been demonstrated that the proposed SM structure can perform the start-up process successfully for automotive applications.

Shutdown procedure

During the Shutdown procedure, the same SM communication strategy is followed as in the start-up procedure. The state machine sends the protocol numbers and setpoints to the subsystem controllers in order to shut down the different subsystems. The shutdown procedure is shown in Fig. 4(b). It indicates how the various operation modes of the subsystems are enabled through the protocol numbers. The condition for transitioning from one substate such as 'Cathode Max flow' to the next substate, 'Cathode min flow' is indicated on the arrows leading from initial state to the final state. If the conditions are not met, the SM will stay in the previous substate and the 'Failsafe' is triggered within a given time frame. Fig. 5 shows the activation signals for $t > 540$ s of a normal shutdown, and how the subsystems are shut down based on the programmed shutdown procedure. Moreover, it shows two measurements variables, namely the air mass flow and the inlet coolant temperature. The air mass flow decreases when the protocol number of cathode changes from 4 to 1, then increases to a maximum value of $50(g/s)$ for protocol number = 5 at $t = 550$ s to dry the stack.

In this test, the stack temperature setpoint is $T\_stack \approx 69°C$ and the 'Cooling loop' was activated in the thermal subsystem with protocol number = 3 and then at $t = 546$ s, the setpoint of the inlet coolant is set to 60°C as the shutdown temperature to cools down the stack. The inlet coolant temperature decreases, resulting in a corresponding decrease in

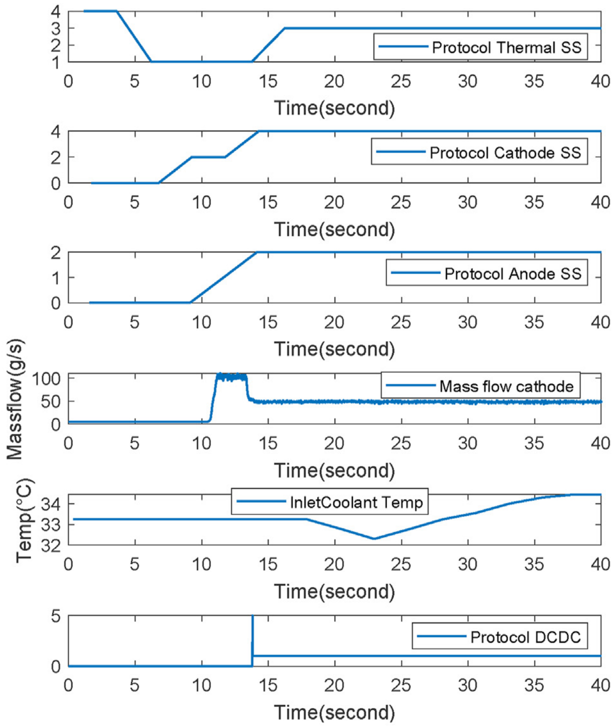

(a) Activation of subsystems in the Start-up procedure

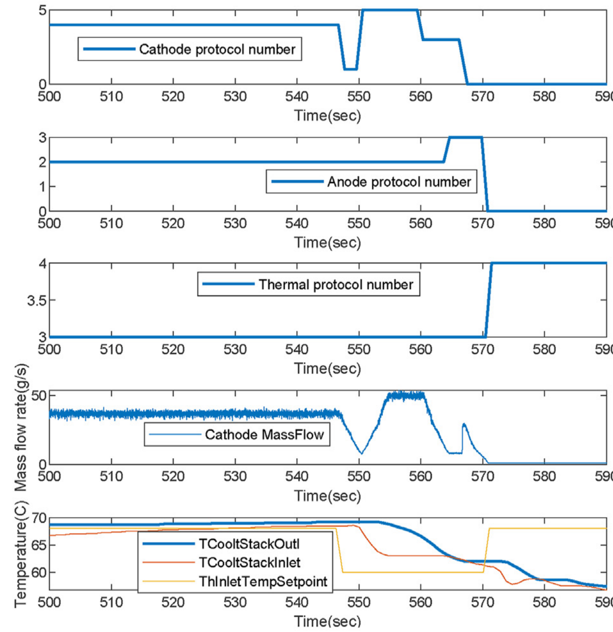

(b) Activation of subsystems in the Shutdown procedure

Fig. 5 – Measured activation signal, protocol number, of the subsystems in Startup and Shutdown procedure.

(a) Vehicle rig at Chalmers University

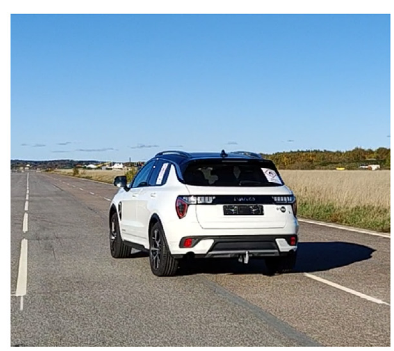

(b) CEVT Proving Ground

Fig. 6 – Prototype fuel cell electric vehicle that was tested in Chalmers University and CEVT facilities [33].

the outlet coolant temperature, and eventually reaching a safe shutdown temperature. Based on the experimental results presented in Fig. 5, it has been shown that the proposed SM framework can successfully carry out the fuel cell system processes in a real prototype vehicle. Furthermore, the fuel cell system has a successful start-up and shutdown.

Run state

During the ‘Run’ state, the power demanded by the vehicle is converted into the corresponding current, and the setpoints values are generated based on this current. Furthermore, based on the measurement signals, the Power Limit Calculator computes the DC/DC current setpoint, and the stack available power information.

The SM receives setpoints of the BoP subsystems from the optimal setpoint generator, and the DC/DC current setpoint from Power Limit Calculator. These setpoints are then sent to the relevant subsystems and DC/DC converter. Additional information regarding this can be found in the section Automotive run state test and experimental results.

Optimal setpoint generator

Considering the issues that arise as a result of operating in an adverse operating point, it is important to find the optimal operating condition for each load power and keep the fuel cell system working in that condition. The operation conditions include inlet air pressure, mass flow rate and humidity ratio, hydrogen pressure, and stack temperature. These operating conditions are specified as the setpoints for the different subsystems. The subsystem controllers keep track of and ensure that these setpoints are being maintained. The optimal setpoint generator is a part inside the supervisory controller that is executed during the 'Run' state, and generates these optimal operation conditions. The generated setpoints are delivered to the state machine as shown in Fig. 7. It is important to note that during other states of operation such as the 'Startup' and 'Shutdown', the subsystem local controller setpoints are defined inside the State Machine based on the practical and manufacturing requirements. The State Machine as the central part of the fuel cell supervisory controller feeds these setpoints to the subsystem local controllers during the different states of operation. As the computational burden is important in implementing algorithms or controllers in automotive applications, an offline optimal setpoint generator in the form of an offline map was proposed and implemented in this project. MPC could achieve online optimized solutions, however, the real-time operation of the MPC presented in the literature is still not possible due to the high computation time [30]. The optimal setpoint generator determines the optimal setpoints corresponding to each load power, thereby maximizing the efficiency of the fuel cell system. Firstly, the requested load power is converted into the corresponding current using an offline map. This current value is then utilized as an input to the optimal setpoint generator, which in turn calculates the optimal setpoints. More details about the optimal setpoint generator can be found in the previous work [31]. PEMFC efficiency, which is defined as the ratio of the net generated power to the enthalpy of reaction of the fed hydrogen, is computed as follows:

$$\eta = \frac{P_{net}}{HHV \cdot \dot{n}_{H_2}} = \frac{IV_{fc} - \sum_{s=subsystems} P_s}{HHV \cdot \dot{n}_{H_2}} \tag{1}$$

where $\dot{n}_{H_2}$ is the fuel out of the H_2 tank, and the HHV the higher heating value of hydrogen. IV_{fc} is the gross electrical power generated by the fuel cell and P_s is the electrical power consumed by the subsystems. The optimal setpoints corresponding to the load current are shown in Table 2.

Power limit calculator

One of the functionalities of the FCSSC is to compute the fuel cell stack's available power range, which is then sent to the

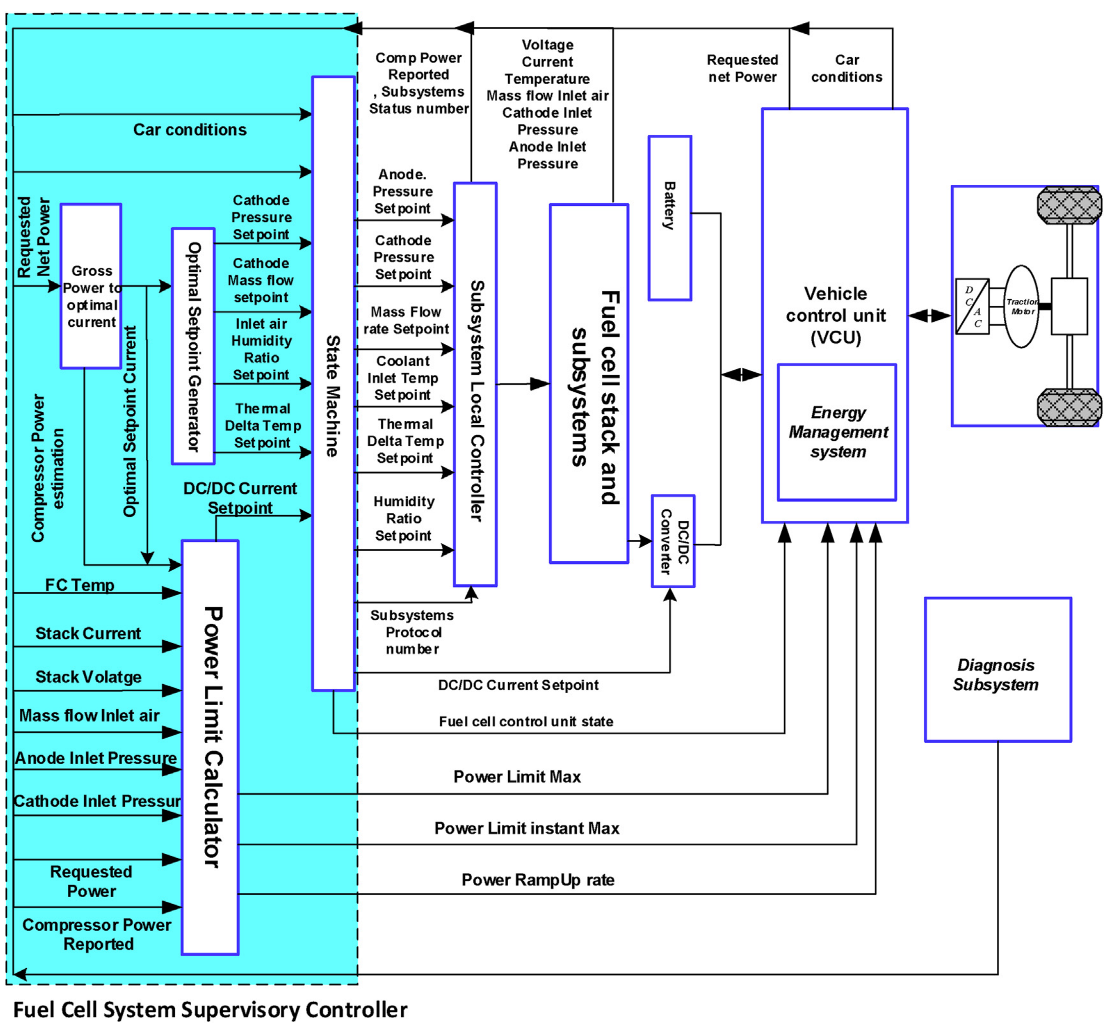

Fig. 7 – Block diagram of the proposed FCSSC integrated with the automotive fuel cell system.

Table 2 – Optimal setpoints values of the different parameters corresponding to the stack current.

Current	$r_1 = \dot{m}_{cathode}$	$r_2 = p_{cathode}$	$r_3 = h_r$	$r_4 = p_{anode}$	$r_5 = T_{in}$	$r_6 = \Delta T_{thermal}$
60	25.68	1.18	0.12	0.2	68	2
100	28.15	1.28	0.12	0.2	68	2
150	34.49	1.39	0.12	0.2	68	4
200	48.098	1.61	0.12	0.2	68	8
250	56.047	1.63	0.12	0.2	68	10
300	66.82	1.75	0.12	0.2	68	12
350	75.91	1.95	0.095	0.2	68	12
400	86.45	1.97	0.095	0.2	68	12
450	94.83	2.08	0.07	0.2	68	12

vehicle control unit's energy management system for effective power distribution. The energy management system uses this information to manage the power requested by the traction components between the fuel cell stack system and the battery. The information that the FCSSC delivers to the energy management system are as follows: Maximum power, Maximum power ramp-up rate, Maximum instant power, and DC-DC set-point current. Using this information, the power requested to the fuel cell system is kept within the capability of the system, which is crucial to minimize stack degradation and/or damage. In the following sections, more details about each output calculation are presented.

Maximum power

The maximum power refers to the maximum net power that the fuel cell is expected to be able to deliver given enough time to change the fluid dynamic state. It depends on the current stack temperature and membrane hydration conditions, and its value will be used to limit the power required by the fuel cell system. Due to the slow dynamics of the stack temperature and the hydration conditions compared with the dynamics of the air compressor, the settling time of stack temperature and hydration condition are larger than the settling time constants of inlet air pressure and mass flow rate, which are smaller than 3 s. The only parameters that affect the maximum power are the stack temperature and the hydration conditions, represented by the Electrochemically Active Surface Area (ECSA). The ECSA is a measure of the total active Pt available in the carbon-support layer at the cathode CL (CCL). It is influenced by various factors, including the Pt loading of the CCL, the pore distribution, the degradation condition of the stack, and the hydration level of the CCL [32]. The hydration level of the CCL changes in dynamic load profile such as the one in automotive applications. Consequently, the ECSA could be and is chosen as an effective index to show the hydration state of the stack. In this work, Eq. (2) is obtained using the experimentally validated stack model detailed in Ref. [32].

$$P(T, ECSA) = 59410 + 36520\,T + 2906\,ECSA + 2690\,T^2 + 654.6\,T \times ECSA - 424.3\,ECSA^2 \quad (2)$$

Where, the ECSA and the stack temperature T are the inputs and the maximum stack gross power is the output. More information about the ECSA and its estimation are detailed in Ref. [32].

Maximum power ramp-up rate

To obtain the maximum ramp-up rate of power at each instant of time, the following calculation is used:

$$\frac{\Delta P}{\Delta t} = \frac{P_2 - P_1}{\Delta t} \quad (3)$$

where P_2 is the maximum power point at the measured stack temperature and the humidity conditions, and it is obtained using Eq. (2), and P_1 is the measured power. By applying equation (2) along with the measured stack current and voltage, one has

$$P_2 = P(T, ECSA) \quad (4)$$

$$P_1 = V_1 I_1 = V_{stack} I_{stack} \quad (5)$$

The calculation of Δt is given by

$$\Delta t \approx \frac{I_2 - I_1}{\frac{dI(t)}{dt}} \quad (6)$$

Considering the technical characteristics of the stack, the minimum permissible output voltage of the stack given at maximum power is $V_2 = 220$. Therefore, the current at maximum power point can be calculated as follows:

$$I_2 = \frac{P_2}{V_2} = \frac{P(T, ECSA)}{220} \quad (7)$$

Based on the relationship between the stack current and the mass flow rate of inlet oxygen, in Eq. (8) $\frac{dI(t)}{dt}$ can be calculated. Regarding the information contained in the compressor's datasheet, the maximum mass flow rate of the compressor is $max(\frac{d\dot{m}_{in}}{dt}) \approx 66(g/s^2)$. Considering Eq. (8) and the maximum mass flow rate of the compressor, the change of current relative to time is given by

$$\frac{dI(t)}{dt} = \frac{d\dot{m}_{O_{2in}}}{dt} \frac{4F}{M_{O_2} n_c} \frac{1}{\lambda_{O_2}} \quad (8)$$

Now, Δt can be calculated using Eq. (6), and the maximum power ramp-up rate is given by Eq. (3)

Maximum instant power

Maximum instant power refers to the maximum net power that the system can deliver in the next sampling time (0,01s). Maximum instant power can be calculated based on the estimation of the maximum safe current that can be drawn from the stack in the next sampling time, as well as the stack voltage in the next sampling time. The maximum safe current is equal to the DC-DC set-point current that will be explained in section DC-DC set-point current. The stack voltage in the next sampling time is equal to the measured stack voltage at the current time, subtracted by the voltage drop caused by activation loss, impedance losses, and concentration losses. So, the Maximum instant net power is calculated as Eq. (9) and Eq. (10)

$$P_{instantMax} = V_{nxtInst} \cdot (I_{dc-dc}) - P_{loss} \tag{9}$$

$$V_{nxtInst} = V_{measurment} - \Delta V_{Activation} - \Delta V_{Impedance} - \Delta V_{Concentration} \tag{10}$$

where $P_{instantMax}$ is the estimation of the maximum net power that the stack can deliver in the next sampling time $(k+1)T_s$; $V_{nxtInst}$ is the estimation of stack voltage in the next sampling time $(k+1)T_s$. The compressor consumption as the lost power is considered in P_{loss}. The impedance loss $\Delta V_{Impedance}$ is calculated as Eq. (11)

$$\Delta V_{Impedance} = R_{ohm}(I_{dc-dc} - I_{stack}) \tag{11}$$

where R_{ohm} is the Ohmic resistance of the stack obtained based on the validated model. I_{stack} and I_{dc-dc} are the stack-measured current and DC-DC setpoint current, respectively. The sampling time of the control system is 10 ms and a small change in the current is expected in this short time. Since the system is operating in the linear region of the polarization curve, it was assumed that the change in voltage from one sampling time to the next is due only to the Ohmic voltage drop. This is a good assumption because of the way the estimated stack voltage in the next sampling time is calculated in Eq. (10), where the fuel cell losses are subtracted from the measured voltage of the previous time step. The changes in activation and concentration losses in the linear region are considered negligible.

DC-DC set-point current

The fuel cell system supervisory controller estimates the safe current to be drawn from the stack. In automotive applications, fuel cells are exposed to challenging scenarios of rapid load changes [20]. Therefore, due to the compressor's dynamic behavior, air starvation is possible, and consequently, stack degradation can occur. In order to prevent damage to the stack caused by a sudden change of load current, which could result in air starvation and increased fuel cell degradation, it is necessary to measure the amount of inlet air to the stack at regular intervals. By using this measurement, the maximum safe current that can be drawn from the stack can be determined. Therefore, the fuel cell supervisory controller ensures that the drawn load current is the safe current that the stack can provide. This safe current which is the DC/DC converter setpoint is calculated as follows.

$$I_{dc-dc}(t) = \frac{\dot{m}_{total} 4F}{M_{dryair} n_c} \times \frac{0.2095}{(1+HR)\lambda_{O_2}} \tag{12}$$

where $\dot{m}_{total}$ is the measured inlet mass flow rate, and the HR is the ambient humidity ratio before the humidifier. The stoichiometry λ_{O2} is set to the minimum permissible stoichiometry.

Automotive run state test and experimental results

In this section, the purpose is to implement the proposed supervisory controller in an automotive proton-exchange membrane (PEM) fuel cell system (FCS). Several tests were performed on the integrated system in order to evaluate the performance, functionalities and durability of the FCS. After, the evaluation of the FCS at PowerCell Sweden facilities, the FCS was integrated into a vehicle platform to test the performance and drivability under automotive conditions. The automotive conditions tests were conducted in a vehicle rig at Chalmers University of Technology, and in proving ground test at China Euro Vehicle Technology (CEVT) facilities, as shown in Fig. 6.

This section will describe and evaluate the performance of proposed fuel cell supervisory controller in the Run state. As stated in section SM cycle, there are ten discrete states for the fuel cell system. It is assumed that the fuel cell system is already in the Run state at the beginning of this analysis. During the Run state, the optimum setpoint generator updates the subsystems' setpoints based on the requested gross power from the vehicle side. During the Run state, the SM receives subsystems setpoints from the optimal set-point generator and the DC/DC setpoint current from the power limit calculator, and then sends them to the appropriate subsystems and DC/DC converter. The block diagram of the FCSSC integrated with the other auxiliary subsystems, namely anode, cathode, thermal, FC stack, vehicle control unit, propulsion parts, and diagnosis subsystem is shown in Fig. 7. In the Run state, the following procedure is conducted at each iteration of the controller operation, i.e., every 0.01 s.

- According to the driver acceleration decision, the signal of the net power requested by the traction motor is generated.
- According to the net power requested by the traction motor, the state of charge of the battery and the implemented energy management algorithm, the vehicle control unit sends the net power request to the fuel cell system.

  Using the compressor power consumption map, the compressor con-sumption is estimated, and it is added to the requested net power to have the gross requested power.

$$P_{gross} = P_{net} + P_{compressor} \tag{13}$$

- The gross power requested is converted into current using the static polarization curve of the stack.
- The optimal setpoints corresponding to the load current for the anode, cathode, and thermal subsystems are generated inside the Optimal setpoint Generator.
- The generated optimal setpoints of the three subsystems are sent to the subsystems' local controllers through the state machine.
- The Power Limit Calculator unit computes the maximum power, the maximum power ramp-up rate, and the maximum instant power by taking into account the stack temperature, stack hydration status, voltage, current, and the estimation power loss due to components such as compressor and fans as explained in section Power limit calculator. The Power Limit Calculator unit directly sends this information as the stack net available power information to the vehicle control unit. Furthermore, the DC/DC converter setpoint current is calculated inside the Limit Power Calculator, and the state machine sends this information to the DC/DC converter as the current setpoint.

Please cite this article as: Molavi A et al., State machine-based architecture to control system processes in a hybrid fuel cell electric vehicle, International Journal of Hydrogen Energy, https://doi.org/10.1016/j.ijhydene.2023.07.039

Table 3 – Base fuel cell electric vehicle specifications.

Engine	Transmission	Curb weight (kgs)		
		Front	Rear	Total
Geely Engine Petrol 3 (GEP3) Max torque: 265 N, Max power: 132 kW	Hybrid 7 Dual Clutch Transmission (7DCTH) Max Torque: 164 Nm, Electrical power: 60 kW	1043	772	1815

Experimental results

In this section, the experimental results of the vehicle on the road for a standard driving cycle are presented. The test was carried out to assess the performance of the whole system in terms of produced power, load profile tracking, and the performance of the balance of plant subsystems local controllers. Driving cycles address the change of speed within a designated timeframe, and its principal characteristics include the duration, average speed, maximum speed, as well as the idling period, acceleration, deceleration, and consistent speed conditions. The Worldwide harmonized Light vehicles Test Cycles (WLTC), which are chassis dynamometer tests for the determination of emissions and fuel consumption from light-duty vehicles, are used in this work. These driving cycles are commonly used in the automotive industry to evaluate the performance of the employed technology in the vehicle. Specifications of the used base vehicle are summarized in Table 3. The powertrain includes a High Voltage (HV) battery, with a total pack energy of 9.7 kWh at the beginning of life and peak power of 75 kW. The HV battery used in this prototype vehicle allows for different power split algorithms between the battery and FC. The split algorithm is implemented inside EMS.

Validation of stack model with experimental data

The measured stack current and the subsystem setpoints are used in Simulink to validate the stack and subsystems model, and the subsystem local controller. Fig. 8 shows the output gross power of the stack in the experimental setup and simulated model. The enlarged time interval between $t = 550$ s to $t = 700$ s, reveals that the Simulink model output power, green line, follows the dynamic behavior of the real output power, blue line, with good precision. It is worth noting that the real output power is gross power, and includes the compressor consumption as well. Therefore, there is a difference between the requested net power and the produced gross power.

Stack output power

The net power requested by the vehicle and the produced gross power of the stack are shown in Fig. 9(a). The magnified timeframe between $t = 600$ s to $t = 800$ s, shows that the fuel cell stack is able to supply the net power requested by the vehicle and to keep up with the load's dynamic. The difference between the produced gross power and the requested net power is the auxiliary power consumption (mainly due to the

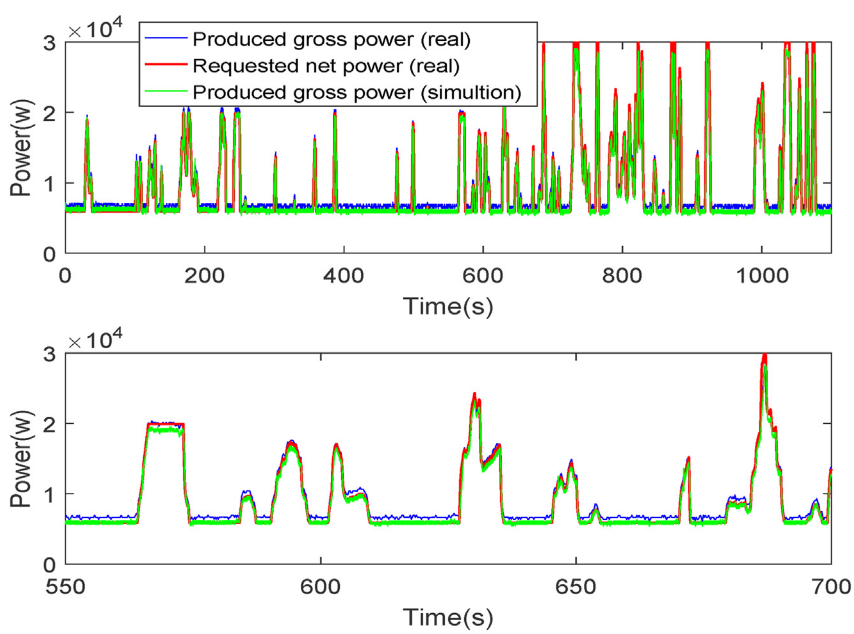

Fig. 8 – Output gross power of the real stack, requested net power, which is the sum of the requested gross power and estimation of compressor loss, in comparison with the output power of the Simulink model, and the zoomed part between t = 550 s to t = 700s.

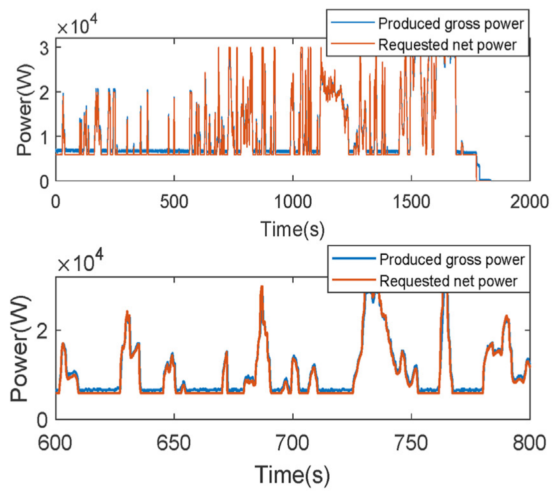

(a) Net power requested by the vehicle and the produced gross power and the zoomed part between $t = 600$ s to $t = 800$ s

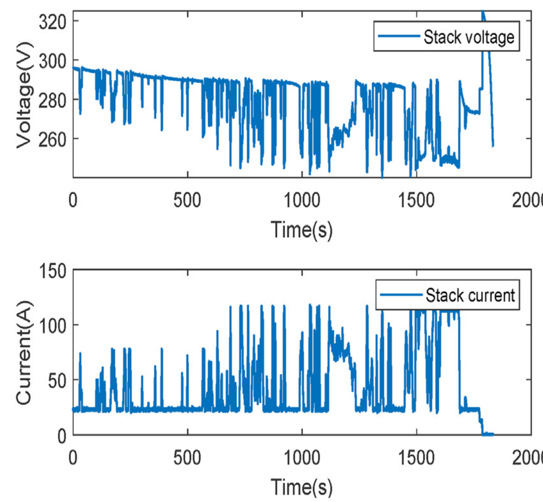

(b) Stack voltage and current

Fig. 9 – Fuel cell Stack output measurements that show the tracking of the dynamic and value of the requested net power in the experimental test.

compressor) that the stack provides. As outlined in the Run state procedure, the initial step involves converting the requested net power into requested gross power, after which the setpoints are determined based on the requested gross power. Therefore, the produced gross power is more than the requested net power as expected. The Stack voltage and current are shown in Fig. 9(b).

Subsystems local controllers' performance

This section will cover the results of the experiments carried out to assess the local controller's performance in achieving setpoints. Considering the requirements of the project, three setpoints are defined for the cathode subsystem. Three setpoints, namely the inlet air mass flow rate, inlet air pressure and humidity ratio, are generated by the optimal setpoint generator and sent to the cathode local controller. The pressure and inlet air humidity ratio setpoints were set to a constant value 1.13 bar and 0.04, respectively. According to Fig. 10, the cathode subsystem local controller effectively tracks the setpoints generated by the optimal setpoint generator.The thermal subsystem was designed and delivered by DLR. The main aspect for evaluation is how well the thermal subsystem is able to control the stack inlet coolant temperature and the outlet coolant temperature, or alternatively, the temperature difference between the inlet and outlet coolant. The experimental results are shown in Fig. 11(a). It turns out that the thermal subsystem effectively controls the stack inlet coolant temperature and the stack outlet coolant temperature, although, the control parameters are dependent of each other.

The anode subsystem was developed by the AVL, and it uses an injector-ejector to control the fuel pressure and increase the hydrogen utilization rate through recirculation. The anode subsystem local controller regulates the anode channel inlet hydrogen pressure and the purge rate in the anode loop. The pressure of the anode has to be controlled at a fixed value above the cathode inlet pressure based on the requirement of the project and the stack safety. The anode inlet pressure and the hydrogen flow from the tank are shown in Fig. 11(b).

Fuel cell system efficiency

To measure and evaluate the efficiency of the system, the consumed hydrogen needs to be measured. The stack and fuel cell system efficiency are calculated as Eq. (1). The subsystems' power consumption of the compressor and fan is considered as the power loss to the fuel cell system. The fuel cell system efficiency considering the lower heating value of hydrogen (120 MJ/kg) and the lost power, is shown in Fig. 12, and it is around 56%. The lower heating value is considered because the state of the water exhaust of a PEM fuel cell stack is mostly vapor. Due to the increase in the load current during this experimental time frame, the efficiency is decreasing.

Software implementation guidelines

The INN-BALANCE project utilized FCCU hardware that was provided by AVL. To facilitate communication and programming of the device, it was necessary to employ the INCA[5]™/EHOOKS™ interface software. This interface software offered several features including revision control, software download, data acquisition, calibration, and real-time monitoring. In order to utilize these features, the required Windows software packages were installed and an

[5] Integrated Calibration and Application Tool, ETAS.

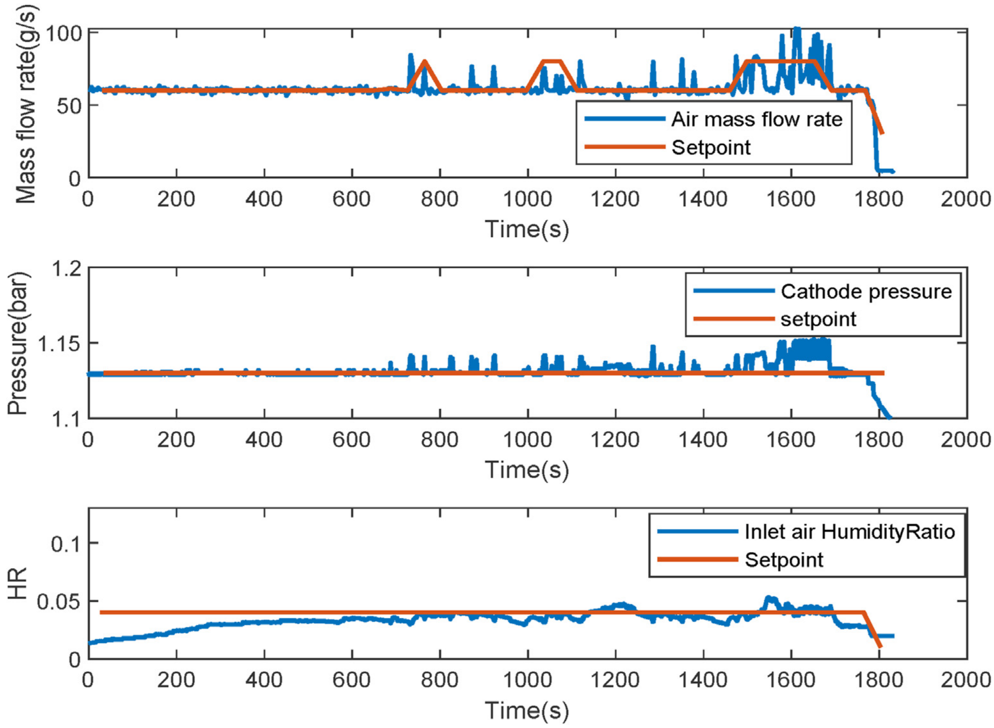

Fig. 10 – Performance of the cathode subsystem local controller to tracks the three setpoints of mass flow rate, pressure, and inlet air humidity ratio in the real-world car vehicle test.

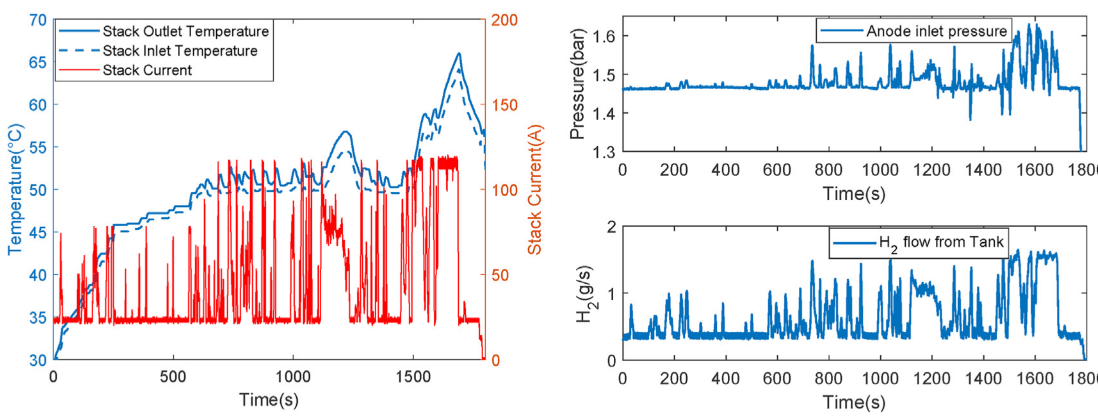

(a) Thermal subsystem coolant inlet and outlet (b) Anode inlet pressure and hydrogen flow

Fig. 11 – Anode and Thermal subsystem measurement parameters.

INCA project was set up. Following this, component commissioning was conducted and all sensors and actuators were tested to ensure proper functionality. The initial start-up was performed gradually, with each step being tested and evaluated before the next step was initiated. Once the start-up process was successfully verified, the functionalities of all subsystems were tested together. One of the critical aspects of the test bed was to evaluate the safety of the fuel cell system in its current form for integration into a vehicle. To mitigate any risks associated with high-voltage vehicle applications, the high-voltage system was galvanically isolated from the chassis ground. Finally, the fuel cell system was integrated under the vehicle hood after its return from laboratory testing. The project required a sampling time of 0.01 s, and the proposed fuel cell control system was capable of executing within this timeframe. This was achieved through the use of lookup tables, which minimized the computational burden. These lookup tables were used to create offline-generated maps that were subsequently uploaded to the control hardware.

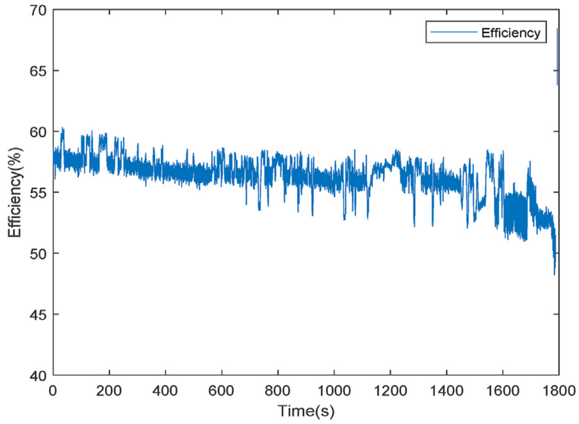

Fig. 12 – Fuel cell system efficiency considering the lower heating value of hydrogen(LHV) which is around 56%.

Conclusion

This work aimed to design, implement, and validate a PEM fuel cell system supervisory controller for an automotive application using the INN-BALANCE developed prototype vehicle at the PowerCell and CEVT facilities. The proposed fuel cell supervisory controller consists of three main components: a state machine, an optimal setpoint generator, and a power limit calculator. The Worldwide Harmonized Light Vehicles Test Cycles (WLTC) were utilized to evaluate the fuel cell system's performance, specifically in terms of load power dynamic tracking, subsystem's local controller performance, and successful start-up and shutdown procedures. Additionally, the overall system performance and efficiency were studied. The state machine served as the central part of the supervisory controller, enabling the fuel cell system to perform its startup and shutdown processes effectively, without errors or equipment damage that could be caused by incorrect subsystem activation. The structure of the state machine allows defining multiple controlled flags and timers in different states or substates. Therefore, there are more degree of freedom to deal with the probable unexpected errors. During the testing of the prototype car, the proposed structure, particularly the state machine, made it easy to identify the system's operational status and diagnose any issues during the test procedure. Therefore, the proposed structure is a simple and reliable method for designing a fuel cell supervisory controller for vehicles and can be used in other applications. To test the controller's accuracy and reliability, a previously validated stack model based on experimental data was used during the supervisory controller's development, resulting in a successful implementation in the real car. The experimental results indicated that the subsystem's local controllers were able to track the provided setpoints effectively, and the fuel cell system operated as expected, allowing the output of the power of the system to match the dynamic power requirements and values requested by the vehicle. Future work includes the testing of the whole control system at full power conditions and freezing startup and shutdown.

Declaration of competing interest

The authors declare that they have no known competing financial interests or personal relationships that could have appeared to influence the work reported in this paper.

Acknowledgements

This work was supported in part by the Spanish national project DOVELAR (RTI2018-096001-B-C32, MINECO/FEDER) also in part by the Fuel Cells and Hydrogen 2 Joint Undertaking under Grant INN-BALANCE 735969. This Joint Undertaking receives support from the European Union's Horizon 2020 research and innovation program and Hydrogen Europe and N. ERGHY.

REFERENCES

[1] Wang C, Ricketts M, Soleymani AP, Jankovic J, Waldecker J, Chen J, Xu C. Improved carbon corrosion and platinum dissolution durability in automotive fuel cell startup and shutdown operation. J Electrochem Soc 2021;168(3):034503.
[2] Wang J, Wang H, Fan Y. Techno-economic challenges of fuel cell commercialization. Engineering 2018;4(3):352–60.
[3] Zhao H, Burke AF. Optimization of fuel cell system operating conditions for fuel cell vehicles. J Power Sources 2009;186(2):408–16.
[4] Dyantyi N, Parsons A, Bujlo P, Pasupathi S. Behavioural study of pemfc during start-up/shutdown cycling for aeronautic applications. Materials for Renewable and Sustainable Energy 2019;8:1–8.
[5] Pei P, Chen H. Main factors affecting the lifetime of proton exchange membrane fuel cells in vehicle applications: a review. Appl Energy 2014;125:60–75.
[6] Yu P, Li M, Wang Y, Chen Z. Fuel cell hybrid electric vehicles: a review of topologies and energy management strategies. World Electric Vehicle Journal 2022;13(9):172.
[7] Rasool M, Khan MA, Zou R. A comprehensive analysis of online and offline energy management approaches for optimal performance of fuel cell hybrid electric vehicles. Energies 2023;16(8):3325.
[8] Wang Y, Advani SG, Prasad AK. A comparison of rule-based and model predictive controller-based power management strategies for fuel cell/battery hybrid vehicles considering degradation. Int J Hydrogen Energy 2020;45(58):33948–56.
[9] Sun X, Zhou Y, Huang L, Lian J. A real-time pmp energy management strategy for fuel cell hybrid buses based on driving segment feature recognition. Int J Hydrogen Energy 2021;46(80):39983–40000.
[10] Yue M, Al Masry Z, Jemei S, Zerhouni N. An online prognostics-based health management strategy for fuel cell hybrid electric vehicles. Int J Hydrogen Energy 2021;46(24):13206–18.
[11] Fu Z, Wang H, Tao F, Ji B, Dong Y, Song S. Energy management strategy for fuel cell/battery/ultracapacitor hybrid electric vehicles using deep reinforcement learning with action trimming. IEEE Trans Veh Technol 2022;71(7):7171–85.
[12] Nie Z, Jia Y, Wang W, Chen Z, Outbib R. Co-optimization of speed planning and energy management for intelligent fuel cell hybrid vehicle considering complex traffic conditions. Energy 2022;247:123476.

[13] Sorrentino M, Cirillo V, Nappi L. Development of flexible procedures for co-optimizing design and control of fuel cell hybrid vehicles. Energy Convers Manag 2019;185:537–51.
[14] Fernandez AM, Kandidayeni M, Boulon L, Chaoui H. An adaptive state machine based energy management strategy for a multi-stack fuel cell hybrid electric vehicle. IEEE Trans Veh Technol 2019;69(1):220–34.
[15] Chu T, Xie M, Yu Y, Wang B, Yang D, Li B, Ming P, Zhang C. Experimental study of the influence of dynamic load cycle and operating parameters on the durability of pemfc. Energy 2022;239:122356.
[16] Salva JA, Iranzo A, Rosa F, Tapia E, Lopez E, Isorna F. Optimization of a pem fuel cell operating conditions: obtaining the maximum performance polarization curve. Int J Hydrogen Energy 2016;41(43):19713–23.
[17] Han J, Yu S, Yi S. Oxygen excess ratio control for proton exchange membrane fuel cell using model reference adaptive control. Int J Hydrogen Energy 2019;44(33):18425–37.
[18] Hu D, Wang Y, Li J, Yang Q, Wang J. Investigation of optimal operating temperature for the pemfc and its tracking control for energy saving in vehicle applications. Energy Convers Manag 2021;249:114842.
[19] Li Y, Ma Z, Zheng M, Li D, Lu Z, Xu B. Performance analysis and optimization of a high-temperature pemfc vehicle based on particle swarm optimization algorithm. Membranes 2021;11(9):691.
[20] Zhang T, Wang P, Chen H, Pei P. A review of automotive proton exchange membrane fuel cell degradation under start-stop operating condition. Appl Energy 2018;223:249–62.
[21] Yang X, Sun J, Sun S, Shao Z. An efficient cold start strategy for proton exchange membrane fuel cell stacks. J Power Sources 2022;542:231492.
[22] Amamou A, Kandidayeni M, Boulon L, Kelouwani S. Real time adaptive efficient cold start strategy for proton exchange membrane fuel cells. Appl Energy 2018;216:21–30.
[23] Jiang F, Wang C-Y. Potentiostatic start-up of pemfcs from subzero temperatures. J Electrochem Soc 2008;155(7):B743.
[24] Jiang F, Wang C-Y, Chen KS. Current ramping: a strategy for rapid start-up of pemfcs from subfreezing environment. J Electrochem Soc 2010;157(3):B342.
[25] Du Q, Jia B, Luo Y, Chen J, Zhou Y, Jiao K. Maximum power cold start mode of proton exchange membrane fuel cell. Int J Hydrogen Energy 2014;39(16):8390–400.
[26] Ríos GM, Schirmer J, Gentner C, Kallo J. Efficient thermal management strategies for cold starts of a proton exchange membrane fuel cell system. Appl Energy 2020;279:115813.
[27] Niu H, Ji C, Wang S, Shi M, Zhang H, Liang C. Analysis of the cold start behavior of a polymer electrolyte membrane fuel cell in constant power start-up mode. Int J Energy Res 2021;45(13):19245–64.
[28] Chen H, Zhao X, Zhang T, Pei P. The reactant starvation of the proton exchange membrane fuel cells for vehicular applications: a review. Energy Convers Manag 2019;182:282–98.
[29] Dong Z, Huang X, Dong Y, Zhang Z. Multilayer perception based reinforcement learning supervisory control of energy systems with application to a nuclear steam supply system. Appl Energy 2020;259:114193.
[30] Di Cairano S, Kolmanovsky IV. Real-time optimization and model predictive control for aerospace and automotive applications. In: 2018 annual American control conference. IEEE: ACC); 2018. p. 2392–409.
[31] Gómez JC, Serra M, Husar A. Controller design for polymer electrolyte membrane fuel cell systems for automotive applications. Int J Hydrogen Energy 2021;46(45):23263–78.
[32] Luna J, Usai E, Husar A, Serra M. Enhancing the efficiency and lifetime of a proton exchange membrane fuel cell using nonlinear model-predictive control with nonlinear observation. IEEE Trans Ind Electron 2017;64(8):6649–59.
[33] Haering P, Garcia Campos JM, Mora González C, Kogler M, Molavi A, Sanchez Monreal J, Nordqvist E, Oberholzer G, Ramette D, Montaner Rios G, et al. INN-BALANCE guidebook. In: Improvement of Balance of Plant Components for PEM based automotive fuel cell systems. Steinbeis-Edition; 2021.

Please cite this article as: Molavi A et al., State machine-based architecture to control system processes in a hybrid fuel cell electric vehicle, International Journal of Hydrogen Energy, https://doi.org/10.1016/j.ijhydene.2023.07.039